[Article] www.whxb.pku.edu.cn

In、Sc 掺杂对 $SrTiO_3$ 电子结构和光学性质的影响

贠江妮 张志勇 *
(西北大学信息科学与技术学院, 西安 710127)

摘要: 采用基于密度泛函理论的第一性原理平面波超软赝势计算方法, 研究了 In、Sc *p* 型掺杂对 $SrTiO_3$ 母体化合物稳定性、电子结构和光学性质的影响. 计算结果表明: 掺杂后, $SrIn_{0.125}Ti_{0.875}O_3$ 和 $SrSc_{0.125}Ti_{0.875}O_3$ 的稳定性降低, 体系显示 *p* 型简并半导体特征, 掺杂仅引起杂质原子近邻区域的几何结构发生变化. 同时, $SrIn_{0.125}Ti_{0.875}O_3$ 和 $SrSc_{0.125}Ti_{0.875}O_3$ 体系的光学带隙分别展宽 0.35、0.30 eV, 光学吸收边发生蓝移, 在 1.25–2.00 eV 的能量区间出现新的吸收峰, 该吸收峰与体系 Drude 型自由载流子的激发相关. 此外, $SrIn_{0.125}Ti_{0.875}O_3$ 和 $SrSc_{0.125}Ti_{0.875}O_3$ 体系的可见光透过率有了明显的提高, 在 350–625 nm 波长范围透过率高于 85%. 掺杂原子在费米能级处低的电子态密度限制了跃迁概率和光吸收. 大的禁带宽度、小的跃迁概率和弱的光吸收是 $SrIn_{0.125}Ti_{0.875}O_3$ 和 $SrSc_{0.125}Ti_{0.875}O_3$ 体系具有较高光学透明度的原因.

关键词: 第一性原理计算; $SrTiO_3$; *p* 型掺杂; 电子结构; 光学性质
中图分类号: O641

Effect of In and Sc Doping on the Electronic Structure and Optical Properties of $SrTiO_3$

YUN Jiang-Ni ZHANG Zhi-Yong*
(*School of Information Science and Technology, Northwest University, Xi'an 710127, P. R. China*)

Abstract: The effect of In and Sc *p*-type doping on the structural stability, electronic structure, and optical properties of $SrTiO_3$ was investigated by first-principles calculations of plane wave ultra-soft pseudo-potential based on density functional theory (DFT). The calculated results revealed that the structural stability of $SrTiO_3$ was weakened after In and Sc doping and that the partial substitution of In for Ti (or Sc for Ti) merely resulted in local structural changes around the dopant sites. The doped $SrIn_{0.125}Ti_{0.875}O_3$ and $SrSc_{0.125}Ti_{0.875}O_3$ systems are *p*-type degenerate semiconductors. The optical bandgap was broadened by about 0.35 eV for $SrIn_{0.125}Ti_{0.875}O_3$ and 0.30 eV for $SrSc_{0.125}Ti_{0.875}O_3$. In addition, a noticeable blue-shift of the absorption spectral edge was observed in the two *p*-type doping systems and a new absorption appeared at around 1.25 to 2.00 eV because of the Drude-type behavior of the free-carrier excitation. The optical transmittance of $SrIn_{0.125}Ti_{0.875}O_3$ and $SrSc_{0.125}Ti_{0.875}O_3$ improved significantly after doping and the transmittances were higher than 85% from 350 to 625 nm. The wide bandgap, small transition probability, and weak absorption because of the low partial density of states of impurities in the Fermi level result in $SrIn_{0.125}Ti_{0.875}O_3$ and $SrSc_{0.125}Ti_{0.875}O_3$ being optically transparent.

Key Words: First-principles calculation; $SrTiO_3$; *p*-type doping; Electronic structure; Optical property

Strontium titanate ($SrTiO_3$), a typical perovskite material, has attracted much attention due to its potential applications in the field of oxide devices[1–9]. It can be used as a substrate for the growth of high temperature superconductor thin films[1], as grain

Received: August 19, 2009; Revised: December 1, 2009; Published on Web: December 23, 2009.
*Corresponding author. Email: zhangzy@nwu.edu.cn; Tel: +86-29-88308280.
The project was supported by the Natural Science Foundation of Shaanxi Province, China (2009JM8013) and Northwest University Graduate Innovation and Creativity Funds, China (08YZZ47).
陕西省自然科学基金(2009JM8013)和西北大学研究生创新基金(08YZZ47)资助项目

boundary barrier layer capacitors[2] and oxygen gas sensors[3–4], and as a high permittivity material with potential application in dynamic random access memory[5]. In particular, its conductivity can be tuned by controlled doping with impurity atoms[6–9], which has important applications in fabricating devices with multilayer structures such as semiconductor/insulator/semiconductor (S/I/S) and metal/insulator/metal (M/I/M) junctions[10].

The behavior of *n*-type doped $SrTiO_3$ has been widely studied in an attempt to understand the rich variations in physical properties arising from carrier doping[11–18]. However, the achievement of *p*-type doped $SrTiO_3$ is rarely documented. Until now, only Sc-doped and In-doped $SrTiO_3$ are confirmed to be *p*-type doping[19–21]. Higuchi *et al*.[19] reported the electronic structure of a *p*-type $SrTiO_3$ single crystal in which the acceptor ion Sc^{3+} was introduced into the Ti^{4+} site. Dai *et al*.[20] reported that $SrTiO_3$ exhibited *p*-type conductivity when doped by the substitution of In for Ti. Guo *et al*.[21] further explored the optical properties of *p*-type $SrIn_xTi_{1-x}O_3$ (x=0.1 and 0.2) films prepared by laser molecular beam epitaxy under different oxygen pressures. In addition, many of the properties such as the structure stability, transport properties, and optical absorption spectra for *p*-type doped $SrTiO_3$ thin films are not known.

In this paper, we perform the first-principles calculation based on the density functional theory (DFT)[22] to investigate the effect of In and Sc *p*-type doping on the electronic structure and optical properties of $SrTiO_3$.

1 Theoretical model and computational method

1.1 Theoretical model

$SrTiO_3$ has an ideal cubic perovskite-type structure at room temperature. It belongs to the space group $Pm3m(O_h)$, with the Sr atom sitting at the origin point, Ti at the body centre, and three oxygen atoms at the three face centres, and its lattice constant is a=b=c=0.3905 nm. The unit cell contains one formula unit of $SrTiO_3$. In order to study fractional substitution, it is necessary to consider a cell larger than the basic unit. Thus we construct a supercell of eight unit cells consisting of 40 atoms in the basis. Replacing any one of the Ti atoms by In (or Sc) atom in the supercell will correspond to the formula $SrIn_{0.125}Ti_{0.875}O_3$ (or $SrSc_{0.125}Ti_{0.875}O_3$).

1.2 Computational method

In our computation, the interaction between nuclei and electrons is approximated with Vanderbilt ultra-soft pseudo-potential[23] treating 4*s*, 4*p*, and 5*s* electrons of Sr, 3*s*, 3*p*, 3*d*, and 4*s* electrons of Ti, 2*s* and 2*p* electrons of O, 4*d*, 5*s* and 5*p* electrons of In, and 3*s*, 3*p*, 3*d*, and 4*s* electrons of Sc as the valence electrons. The Perdew and Wang 91 parametrization[24] is taken as the exchange-correlation potential in the generalized-gradient approximation (GGA). Plane wave basis with kinetic energy cutoff of 420 eV is used to represent wave functions. Brillouin zone integration is performed with a 6×6×6 Monkhorst-Pack[25] *k*-points mesh. Full relaxation is performed for the constructed supercells by using the Broyden-Fletcher-Goldfarb-Shanno (BFGS) algorithm[26] to minimize energy respect to atomic position. Each calculation is considered converged when the maximum root-mean-square convergent tolerance is less than 5.0×10^{-6} eV·atom^{-1}, that is, the maximum ionic Hellmann-Feynman force being within 0.1 eV·nm^{-1}, the maximum ionic displacement being within 5.0×10^{-5} nm and the maximum stress being within 0.02 GPa. Then the electronic structure and optical properties are calculated based on the optimized supercell model.

The scissor approximation is adopted in the optical calculation to compensate the underestimation of the calculated band gap.

2 Results and discussion

2.1 Stability and lattice properties

The binding intensity and structural stability of crystal are related to its binding energy. The bigger the binding energy, the more stable the crystal structure. In this paper, the binding energies for $SrTiO_3$, $SrIn_{0.125}Ti_{0.875}O_3$, and $SrSc_{0.125}Ti_{0.875}O_3$ are calculated by the following formulas[27]:

$$E_b(SrTiO_3)=[E_{total}(SrTiO_3)-nE_{isolate}(Sr)-nE_{isolate}(Ti)-3nE_{isolate}(O)]/n \quad (1)$$

$$E_b(SrM_{0.125}Ti_{0.875}O_3)=[E_{total}(SrM_{0.125}Ti_{0.875}O_3)-nE_{isolate}(Sr)-(n-1)E_{isolate}(Ti)-E_{isolate}(M)-3nE_{isolate}(O)]/n \quad (2)$$

where $E_{total}(SrTiO_3)$ and $E_{total}(SrM_{0.125}Ti_{0.875}O_3)$ represent the total energies of the $SrTiO_3$ and $SrM_{0.125}Ti_{0.875}O_4$ supercells, respectively. $E_{isolate}(X)$ denotes the total energy of an isolated X atom and n is the formula number of $SrTiO_3$ contained in each supercell.

By analysis of the calculated binding energies of the three compounds listed in Table1, we conclude that the optimized $SrTiO_3$, $SrIn_{0.125}Ti_{0.875}O_3$, and $SrSc_{0.125}Ti_{0.875}O_3$ systems are stable, because their binding energies are negative. On the other hand, the doped $SrIn_{0.125}Ti_{0.875}O_3$ and $SrSc_{0.125}Ti_{0.875}O_3$ have bigger binding energy values than the undoped $SrTiO_3$ itself, which indicates that the structure stability of $SrTiO_3$ is weakened after doping. These structure stability changes for $SrIn_{0.125}Ti_{0.875}O_3$ and $SrSc_{0.125}Ti_{0.875}O_3$ are originated from the electronic structure changes through doping, and we will discuss this in the Mulliken population analysis section. Note that the crystal structures of $SrIn_{0.125}Ti_{0.875}O_3$ and $SrSc_{0.125}Ti_{0.875}O_3$ are still the cubic perovskite-type structure with the space group $Pm3m(O_h)$.

In addition, the calculated lattice constants are 0.3951 nm for $SrIn_{0.125}Ti_{0.875}O_3$, larger than that of undoped $SrTiO_3$ (0.3924 nm), which is in good agreement with the experiment results[20] that the

Table 1 Optimized structure parameters and binding energies (E_b) for $SrTiO_3$, $SrIn_{0.125}Ti_{0.875}O_3$, and $SrSc_{0.125}Ti_{0.875}O_3$

System	Space group	a/nm		E_b/eV
		calc.	expt.	calc.
$SrTiO_3$	$Pm3m$	0.3924	0.3905[28]	–42.8037
$SrIn_{0.125}Ti_{0.875}O_3$	$Pm3m$	0.3951	0.3948[20]	–42.1885
$SrSc_{0.125}Ti_{0.875}O_3$	$Pm3m$	0.3948	–	–42.3147

structure parameter a=b=c, so only a is listed.

lattice constants of $SrIn_{0.1}Ti_{0.9}O_3$ films increase after doping. The same lattice expansion tendency is also observed in $SrSc_{0.125}Ti_{0.875}O_3$. However, because of the absence of experimental result on the lattice parameters of $SrSc_{0.125}Ti_{0.875}O_3$, further experimental work is needed for comparison with our numerical results.

Further insight into the effect of *p*-type doping on the electronic structure of $SrTiO_3$ can be obtained from the atomic relaxation around the impurity atom as listed in Table 2. The partial geometries around the impurity In atom, which are taken from the structural optimized $SrIn_{0.125}Ti_{0.875}O_3$ system, are shown in Fig.1.

The introducing of In impurity leads to a local lattice expansion in the $SrIn_{0.125}Ti_{0.875}O_3$. The closest atoms with respect to the In impurity are six O^* atoms which rearrange their positions immediately after the doping has occurred. That is, the six nearest O^* atoms around In atom shift away from In by 0.0025 nm and the InO_6^* octahedron exhibits a small structure relaxation. This is due to the fact that the effective radius of In^{3+}(0.094 nm) is larger than the radius of Ti^{4+}(0.0745 nm)[20], the partial substitution of In for Ti induces a structure relaxation. The same tendency is also observed for $SrSc_{0.125}Ti_{0.875}O_3$ after doping. However, the six nearest O^* atoms around Sc atom move away from Sc by 0.0083 nm, much larger than that in $SrIn_{0.125}Ti_{0.875}O_3$. Furthermore, in the case of the first nearest neighbor (NN) Ti^*O_6 with respect to the InO_6^* octahedron in $SrIn_{0.125}Ti_{0.875}O_3$, it possesses a slightly distorted Ti^*O_6 octahedron. The bond length of Ti^*—O_a along the *a*-axis is smaller than those in the *bc* plane. So does the first NN Ti^*O_6 with respect to the ScO_6 octahedron in $SrSc_{0.125}Ti_{0.875}O_3$. At the same time, it is noted that the second NN $Ti^{**}O_6$ undergoes little relaxations after doping and the third NN $Ti^{\#}O_6$ has almost no change in both $SrIn_{0.125}Ti_{0.875}O_3$ and $SrSc_{0.125}Ti_{0.875}O_3$ systems compared with the corresponding one in the undoped $SrTiO_3$ system. Hence, replacing a Ti atom by one In atom (or Sc atom) in the $SrTiO_3$ parent merely results in local structural changes around the dopant sites.

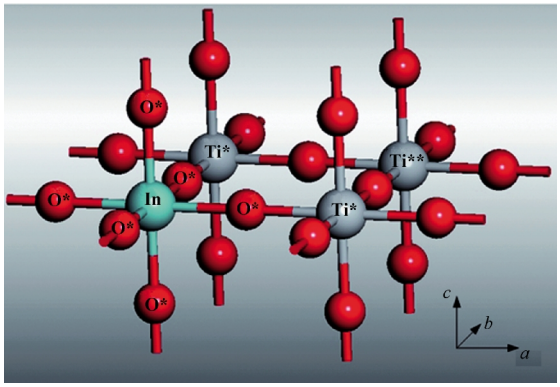

Fig.1 Partial geometry of the structural optimized $SrIn_{0.125}Ti_{0.875}O_3$ system

2.2 Electronic structures

In this part, the electronic structures of $SrTiO_3$, $SrIn_{0.125}Ti_{0.875}O_3$, and $SrSc_{0.125}Ti_{0.875}O_3$ will be discussed and compared with each other. Three indicators will be used to reveal the effect of In and Sc doping on the electronic structure of $SrTiO_3$, which are the total density of state (DOS), partial density of state (PDOS), and population analysis. Each of these tools can demonstrate some aspects of structure features.

2.2.1 DOS

The DOS and PDOS of the undoped $SrTiO_3$ are calculated first for comparison and the results are shown in Fig.2(a). For the sake of clarity, only the relevant Ti 3*d*, O 2*p*, and Sr 5*p* PDOS are shown and this will be adopted in the subsequent figures. It is obvious that the structure of $SrTiO_3$ has corner-shared TiO_6 octahedron where the Ti 3*d* and O 2*p* interaction is found, which dominate the main electronic properties of $SrTiO_3$. The top of valance bands (VBs) predominately consists of O 2*p* states and the most prominent unoccupied energy bands in the bottom most of conduction bands (CBs) are mainly composed of the Ti 3*d* states. Overlooking from the DOS, it can be observed that there is strong orbital hybridization between the Ti 3*d* and O 2*p* states. That is to say, Ti—O bond is covalent. Correspondingly no over-

Table 2 Key bond lengths in $SrTiO_3$, $SrIn_{0.125}Ti_{0.875}O_3$, and $SrSc_{0.125}Ti_{0.875}O_3$

	Undoped $SrTiO_3$		$SrIn_{0.125}Ti_{0.875}O_3$			$SrSc_{0.125}Ti_{0.875}O_3$		
	Bond	Bond length	Bond	Bond length	Δ_1	Bond	Bond length	Δ_2
	Ti—O_a	0.1962	In—O_a^*	0.1987	0.0025	Sc—O_a^*	0.2045	0.0083
	Ti—O_b	0.1962	In—O_b^*	0.1987	0.0025	Sc—O_b^*	0.2045	0.0083
	Ti—O_c	0.1962	In—O_c^*	0.1987	0.0025	Sc—O_c^*	0.2045	0.0083
first NN Ti^*O_6	Ti^*—O_a	0.1962	Ti^*—O_a	0.1937	–0.0025	Ti^*—O_a	0.1903	–0.0059
	Ti^*—O_b	0.1962	Ti^*—O_b	0.1981	0.0019	Ti^*—O_b	0.1985	0.0023
	Ti^*—O_c	0.1962	Ti^*—O_c	0.1981	0.0019	Ti^*—O_c	0.1985	0.0023
second NN $Ti^{**}O_6$	Ti^{**}—O_a	0.1962	Ti^{**}—O_a	0.1968	0.0006	Ti^{**}—O_a	0.1969	0.0007
	Ti^{**}—O_b	0.1962	Ti^{**}—O_b	0.1968	0.0006	Ti^{**}—O_b	0.1969	0.0007
	Ti^{**}—O_c	0.1962	Ti^{**}—O_c	0.1968	0.0006	Ti^{**}—O_c	0.1969	0.0007
third NN $Ti^{\#}O_6$	$Ti^{\#}$—O_a	0.1962	$Ti^{\#}$—O_a	0.1963	0.0001	$Ti^{\#}$—O_a	0.1964	0.0002
	$Ti^{\#}$—O_b	0.1962	$Ti^{\#}$—O_b	0.1963	0.0001	$Ti^{\#}$—O_b	0.1964	0.0002
	$Ti^{\#}$—O_c	0.1962	$Ti^{\#}$—O_c	0.1963	0.0001	$Ti^{\#}$—O_c	0.1964	0.0002

The bond lengths surrounding the impurity In atom in $SrIn_{0.125}Ti_{0.875}O_3$ and the impurity Sc in $SrSc_{0.125}Ti_{0.875}O_3$ are listed. The corresponding bond lengths of undoped $SrTiO_3$ system after structural relaxation are also given for comparison. Δ_1 and Δ_2 denote the bond length changes before and after doping for $SrIn_{0.125}Ti_{0.875}O_3$ and $SrSc_{0.125}Ti_{0.875}O_3$, respectively. Ti^*, Ti^{**}, and $Ti^{\#}$ are the first, second, and third nearest neighbor Ti atoms to the impurity In atom, respectively; O_a, O_b, and O_c are the three different oxygen atoms bonded with Ti atoms. All quantities are in nm.

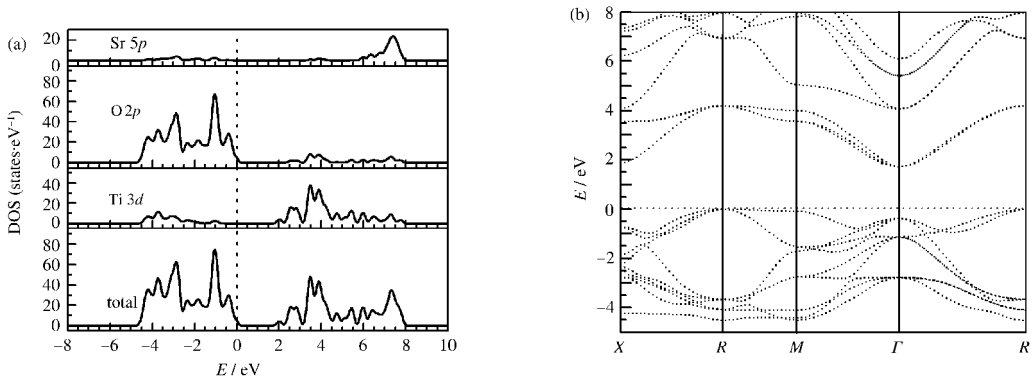

Fig.2 DOS and PDOSs (a) and band structure (b) of undoped $SrTiO_3$

The Fermi level is set to zero on the energy scale, which will be adopted below unless otherwise stated.

lap of PDOS between Sr atoms and O atoms means the high ionicity of Sr—O bonds.

Moreover, as shown in Fig.2(b), the undoped $SrTiO_3$ is an indirect gap insulator with the top of valence band at R point and the bottom of conduction band at Γ point. The calculated value of the indirect band gap at $R \rightarrow \Gamma$ is 1.7 eV, which is smaller than the experimental value of about 3.2 eV[28]. This is typically underestimated by the density functional theory[29–30]. Thus, a scissor approximation value of 1.5 eV is adopted in the optical calculation to compensate the underestimation of the calculated band gap.

Fig.3 shows the total DOSs of $SrIn_{0.125}Ti_{0.875}O_3$ and $SrSc_{0.125}Ti_{0.875}O_3$. Because the In doping introduces the p-type carriers into the $SrIn_{0.125}Ti_{0.875}O_3$ system, the Fermi level shifts into the valence bands (VBs), which is in agreement well with the experimental results[20] that In^{3+} acts as acceptor ions in the Indoped $SrTiO_3$ films and the $SrIn_{0.1}Ti_{0.9}O_3$ is a p-type semiconductor. Particularly, the DOS of $SrIn_{0.125}Ti_{0.875}O_3$ shifts significantly towards high energies and the optical band gap is broadened by about 0.35 eV due to In doping compared with the DOS reported in Fig.2. This is well consistent with the experimental results[20] that the band gap of $SrIn_{0.1}Ti_{0.9}O_3$ is 0.4 eV larger than that of undoped $SrTiO_3$. Moreover, one additional peak with a bandwidth of about 1.20 eV appears in the bottom of VBs for $SrIn_{0.125}Ti_{0.875}O_3$.

In the case of Sc-doped $SrSc_{0.125}Ti_{0.875}O_3$, the Fermi level shifts downwards into the VBs and $SrSc_{0.125}Ti_{0.875}O_3$ exhibits p-type degenerate semiconductor feature, which agree well the experimental results[31] that Sc^{3+} acts as acceptor ions in $SrTi_{1-x}Sc_xO_3$ and the Fermi level shifts to the VBs side with increasing Sc^{3+} ions. Meanwhile, an optical band gap widening of 0.30 eV associated with Sc doping has been observed for $SrSc_{0.125}Ti_{0.875}O_3$. This fact is consistent with the experimental results that the band gap of $SrTi_{1-x}Sc_xO_3$ increases with increasing Sc doping concentration[32]. The broadened optical band gap originates from two aspects. On the one hand, the Burstein-Moss shift due to the high concentration of carriers makes the optical absorption edge shifts towards high energies and the optical transparency window is broadened[33]. On the other hand, interactions among hole charges result in a many-body effect, which causes the optical band gap to become narrow[34]. However, the effect of Burstein-Moss on the band gap is more pronounced than that of the many-body effect, so the band gap broadens after doping.

2.2.2 PDOS

In subsequent discussions on the effect of p-type doping on the $SrTiO_3$ system, we restrict ourselves to the PDOS of the doped systems.

Firstly, the orbital decomposed PDOSs of impurity In atom in $SrIn_{0.125}Ti_{0.875}O_3$ and Sc atom in $SrSc_{0.125}Ti_{0.875}O_3$ are presented in Fig.4(a). It is clear that the PDOSs of In and Sc do not contribute to the bottom most of CBs but contribute only to the top of VBs. The value of PDOS for In near the Fermi level (marked by the arrow in Fig.4(a)) in the energy rang of −0.50 to 0.00 eV is significantly larger than that of Sc atom in $SrSc_{0.125}Ti_{0.875}O_3$. This indicates that In is probably better than Sc for p-type doping in $SrTiO_3$.

Secondly, the orbital decomposed PDOSs of atoms near the In and Sc impurities are plotted in Fig.4 (b) and (c), respectively. In the case of $SrIn_{0.125}Ti_{0.875}O_3$, it is found that there is strong interaction between impurity In and its first NN Ti^*O_6. The PDOS of Ti^* $3d$ states at the bottom of CBs is highly dispersive and shows no localization characteristics. With increasing distance between In and its neighboring TiO_6, the PDOS of Ti^{**} $3d$ states is less dispersive than that of Ti^*. The PDOS of $Ti^{\#}$ atom is almost the same as that in undoped $SrTiO_3$. Besides, the In impurity charge potential has great effect on the six O^* atoms in the InO_6. The PDOS of O^* $2p$ states at the bottom of CBs is different from that of other O atoms, which are not in the InO_6. The same results are observed in $SrSc_{0.125}Ti_{0.875}O_3$. These conclusions for $SrIn_{0.125}Ti_{0.875}O_3$

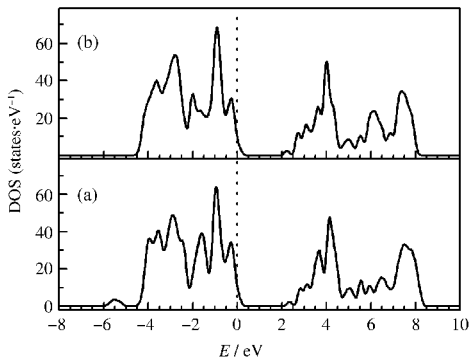

Fig.3 DOSs of $SrIn_{0.125}Ti_{0.875}O_3$ (a) and $SrSc_{0.125}Ti_{0.875}O_3$ (b)

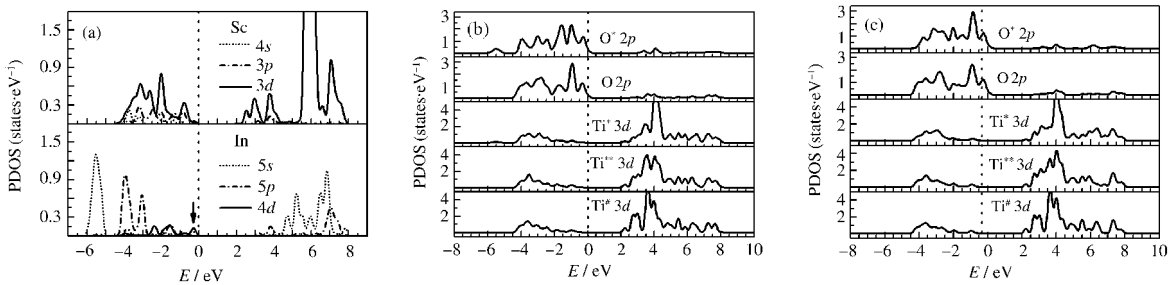

Fig.4 PDOSs of impurity In atom in $SrIn_{0.125}Ti_{0.875}O_3$ and Sc atom in $SrSc_{0.125}Ti_{0.875}O_3$ (a), surrounding atoms of In (b) and neighboring atoms of Sc (c)

and $SrSc_{0.125}Ti_{0.875}O_3$ are in good agreement with the structure relaxation analysis in section 2.1 that the partial substitution of In for Ti (or Sc for Ti) in the $SrTiO_3$ parent merely results in local structural changes around the dopant sites. Moreover, by analysis the PDOS in Fig.4(a,b), it is evident that an additional peak appears in the bottom of VBs for $SrIn_{0.125}Ti_{0.875}O_3$, to which the In 5*s* and O 2*p* states make contribution.

2.2.3 Mulliken population analysis

More investigation of the effect of In and Sc doping on the electronic structure of $SrTiO_3$ can be obtained from Mulliken population analysis listed in Table 3. For undoped $SrTiO_3$, the net charge of Sr (1.87*e*) is close to its +2*e* formal charges, whereas O atom is with –0.80*e* negative charges and Ti atom carries 0.53*e* positive charges, which are much smaller than their –2*e* and +4*e* formal charges, respectively. This indicates that there is a high degree of covalency in the Ti—O bond while ionicity in the Sr—O bond, which agrees well with the DOS analysis for $SrTiO_3$ in section 2.2.1.

After doping, there are considerable electron charge density redistributions near the impurity atom. In the case of $SrIn_{0.125}Ti_{0.875}O_3$, the electron density of the O^* atoms near the impurity In atom increases obviously and the electronegativity of O^* atoms is strengthened. While the net charges of Ti^* and Ti^{**} decrease to the values of 0.50*e* and 0.52*e*, respectively. This is due to the fact that the net charge of In atom (1.26*e*) is much larger than that of the replaced Ti atom (0.53*e*), and In atom transfers more electrons to O^* atoms. Correspondingly, Ti^* and Ti^{**} provide less electrons to O^* atoms. Hence there is a high degree of ionicity in the In—O bond and the covalency of Ti—O bond is weakened after doping, which result in the structure stability change of $SrIn_{0.125}Ti_{0.875}O_3$. For $SrSc_{0.125}Ti_{0.875}O_3$, the impurity Sc atom loses only partial valence electrons with 0.46*e* positive charges, smaller than the replaced Ti atom (0.53*e*), implying that the covalent Sc—O bond is weaker than that of Ti—O bond. Correspondingly, Ti^* and Ti^{**} atoms transfer more electrons to O^* atoms and the net charges of Ti^* and Ti^{**} increase to the values of 0.56*e* and 0.54*e*, respectively.

2.3 Optical properties

Next we discuss the effect of In and Sc doping on the optical properties of $SrTiO_3$. The linear response of a system due to an external electromagnetic field with a small wave vector can be described with the complex dielectric function $\varepsilon(\omega)=\varepsilon_1(\omega)+i\varepsilon_2(\omega)$. The imaginary part of the dielectric function $\varepsilon_2(\omega)$ is calculated from the momentum matrix elements between the occupied and unoccupied wave functions[35] as follows:

$$\varepsilon_2(\omega)=\frac{Ve^2}{2\pi\hbar m^2\omega^2}\int \mathrm{d}^3k\sum_{n,n'}|\langle kn|p|kn'\rangle|^2 f(kn)(1-f(kn'))\delta(E_{kn}-E_{kn'}-\hbar\omega) \quad (3)$$

where $\hbar\omega$ is the energy of the incident photon, V is the unit cell volume, p is the momentum operator, $|kn>$ is a crystal wavefunction, and $f(kn)$ is the Fermi distribution function. The real part of the dielectric function $\varepsilon_1(\omega)$ is evaluated from the imaginary part $\varepsilon_2(\omega)$ by the Kramers-Kronig relationship.

$$\varepsilon_1(\omega)=1+\frac{2}{\pi}M\int_0^\infty \frac{\varepsilon_2(\omega')\omega'}{\omega'^2-\omega^2}\mathrm{d}\omega \quad (4)$$

where M is the principal value of the integral. The other optical constants like refractive index $n(\omega)$, extinction coefficient $k(\omega)$, reflectivity $R(\omega)$, and absorption coefficient $I(\omega)$ now immediately are calculated in terms of the components of the complex dielectric function as follows:

$$n(\omega)=\left(\frac{1}{\sqrt{2}}\right)[\sqrt{\varepsilon_1(\omega)^2+\varepsilon_2(\omega)^2}+\varepsilon_1(\omega)]^{1/2} \quad (5)$$

$$k(\omega)=\left(\frac{1}{\sqrt{2}}\right)[\sqrt{\varepsilon_1(\omega)^2+\varepsilon_2(\omega)^2}-\varepsilon_1(\omega)]^{1/2} \quad (6)$$

$$R=\frac{(n-1)^2+k^2}{(n+1)^2+k^2} \quad (7)$$

$$I=\frac{2K\omega}{c} \quad (8)$$

Accordingly the transmittance $T(\omega)$ can be obtained by the following equation:

$$T(\omega)=1-R(\omega)-I(\omega) \quad (9)$$

Fig.5 shows the absorption spectra for $SrTiO_3$, $SrIn_{0.125}Ti_{0.875}O_3$, and $SrSc_{0.125}Ti_{0.875}O_3$. After doping, a noticeable blue-shift of ab-

Table 3 Mulliken population analysis for $SrTiO_3$, $SrIn_{0.125}Ti_{0.875}O_3$, and $SrSc_{0.125}Ti_{0.87}O_3$

$SrTiO_3$		$SrIn_{0.125}Ti_{0.875}O_3$		$SrSc_{0.125}Ti_{0.875}O_3$	
Ion	Net charge (*e*)	Ion	Net charge (*e*)	Ion	Net charge (*e*)
Sr	1.87	Sr	1.87	Sr	1.87
Ti	0.53	Ti	0.53	Ti	0.53
O	–0.80	O	–0.80	O	–0.80
		In	1.26	Sc	0.46
–	–	Ti^*	0.50	Ti^*	0.56
–	–	Ti^{**}	0.52	Ti^{**}	0.54
		O^*	–0.90	O^*	–0.81

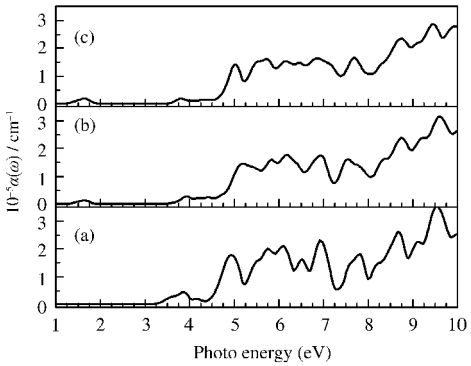

Fig.5 Absorption spectra of $SrTiO_3$ (a), $SrIn_{0.125}Ti_{0.875}O_3$ (b), and $SrSc_{0.125}Ti_{0.875}O_3$ (c)

sorption spectra edge is observed for $SrIn_{0.125}Ti_{0.875}O_3$ and $SrSc_{0.125}Ti_{0.875}O_3$, which is in good agreement with the above calculated optical band gap widening for them. In addition, because of the Drude-type behavior of the free-carrier excitation[12], a new weak absorption appears in the energy region of 1.25 to 2.00 eV for the two *p*-type doping systems.

At the same time, as shown in Fig.6, the optical transmittance of $SrIn_{0.125}Ti_{0.875}O_3$ has a significant improvement after In doping and the transmittance is higher than 85% in a wavelength range from 350 to 625 nm, which agree well with the experimental results[21] that $SrIn_{01}Ti_{09}O_3$ thin films are highly transparent with the transmittance higher than 80% in most of the visible spectrum. For $SrSc_{0.125}Ti_{0.875}O_3$, its optical transmittance is similar to that of $SrIn_{0.125}Ti_{0.875}O_3$.

The increasing of the high transparency of the two *p*-type doping compounds originates from two factors. On one hand, to being optically transparent, it is desirable to have a wider band gap than the photon energy of the visible lights. Owing to the *p*-type doping, there is an optical band gap widening of 0.35 and 0.30 eV for $SrIn_{0.125}Ti_{0.875}O_3$ and $SrSc_{0.125}Ti_{0.875}O_3$, respectively. Therefore, the electron transition occurring above 3.55 eV in $SrIn_{0.125}Ti_{0.875}O_3$ (3.50 eV in $SrSc_{0.125}Ti_{0.875}O_3$) should be more beneficial than the band gap of 3.20 eV[23] in $SrTiO_3$. On the other hand, the PDOS of impurity atom is low in the Fermi level (see Fig.4 (a)), which leads to the small transition probability and weak absorption.

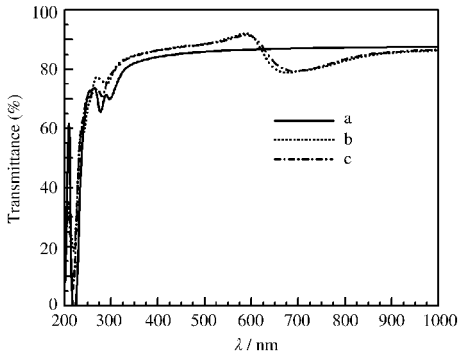

Fig.6 Optical transmittances of $SrTiO_3$ (a), $SrIn_{0.125}Ti_{0.875}O_3$ (b), and $SrSc_{0.125}Ti_{0.875}O_3$ (c)

3 Conclusions

In conclusion, we have investigated the structure stability, electronic structure, and optical properties of In and Sc *p*-type doped $SrTiO_3$ by the first-principles calculation of plane wave ultra-soft pseudo-potential based on the DFT. Our calculation results are in good agreement with the experimental data. From these calculations, we have obtained the results as follows.

(1) The structures of $SrIn_{0.125}Ti_{0.875}O_3$ and $SrSc_{0.125}Ti_{0.875}O_3$ are still stable after doping, but their stabilities are lower than that of undoped $SrTiO_3$.The partial substitution of In for Ti (or Sc for Ti) in the $SrTiO_3$ parent merely results in local structural changes around the dopant sites.

(2) Owing to the *p*-type doping, the Fermi level shifts into VBs for both $SrIn_{0.125}Ti_{0.875}O_3$ and $SrSc_{0.125}Ti_{0.875}O_3$ systems and the two systems display *p*-type degenerate semiconductor features. At the same time, the optical band gap of $SrIn_{0.125}Ti_{0.875}O_3$ is broadened by about 0.35 eV due to In doping and an optical band gap widening of 0.30 eV associated with Sc doping has been observed for $SrSc_{0.125}Ti_{0.875}O_3$.

(3) A noticeable blue-shift of absorption spectra edge is observed for $SrIn_{0.125}Ti_{0.875}O_3$ and $SrSc_{0.125}Ti_{0.875}O_3$ and a new absorption appears in the energy region of 1.25 to 2.00 eV for the two *p*-type doping systems. Furthermore, the optical transmittances of $SrIn_{0.125}Ti_{0.875}O_3$ and $SrSc_{0.125}Ti_{0.875}O_3$ have a significant improvement after doping, and the transmittances are higher than 85% in the wavelength range from 350 to 625 nm. The wide band gap, small transition probability, and weak absorption due to the PDOS of impurity in the Fermi level result in the significant optical transparency.

References

1 Eom, C. B.; Marshall, A. F.; Laderman, S. S.; Jacowitz, R. D.; Geballe, T. H. *Science*, **1990, 249**: 1549

2 Shen, H.; Song, Y.; Gu, H.; Wang, P.; Xi, Y. *Mater. Lett*., **2002, 56**: 802

3 Hara, T.; Ishiguro, T. *Sens. Actuator B-Chem*., **2009, 136**: 489

4 Hara, T.; Ishiguro, T.; Wakiyab, N.; Shinozakic, K. *Mater. Sci. Eng. B*, **2009, 161**: 142

5 Lee, S. W.; Kwon, O. S.; Han, J. H.; Hwang, C. S. *Appl. Phys. Lett*., **2008, 92**: 222903

6 Fix, T.; Bali, R.; Stelmashenko, N.; Blamire, M. G. *Solid State Commun*., **2008, 146**: 428

7 Zhu, X. B.; Liu, S. M.; Hao, H. R.; Li, X. H.; Song, W. H.; Sun, Y. P. *Physica C*, **2005, 418**: 59

8 Higuchi, T.; Tsukamoto, T.; Kobayashi, K.; Ishiwata, Y.; Fujisawa, M.; Yokoya, T.; Yamaguchi, S.; Shin, S. *Phys. Rev. B*, **2000, 61**: 12860

9 Marina, O. A.; Canfield, N. L.; Stevenson, J. W. *Solid State Ionics*, **2002, 149**: 21

10 Wang, H. H., Chen, F.; Dai, S. Y.; Zhao, T.; Lu, H. B.; Cui, D. F.; Zhou, Y. L.; Chen, Z. H.; Yang, G. Z. *Appl. Phys. Lett*., **2001, 78**: 1676

11 Wang, H. H.; Cui, D. F.; Dai, S. Y.; Lu, H. B.; Zhou, Y. L.; Chen, Z. H.; Yang, G. Z. *J. Appl. Phys*., **2001, 90**: 4664

12 Higuchi, T.; Tsukamoto, T.; Taguchi, Y.; Tokur, Y.; Shin, S. *Physica B*, **2004, 351**: 310

13 Ma, J. Y.; Bi, C. Z.; Fang, X.; Zhao, H. Y.; Kamran, M.; Qiu, X. G. *Physica C*, **2007, 463–465**: 107

14 Takizawa, M.; Maekawa, K.; Wadati, H.; Yoshida, T.; Fujimori, A.; Kumigashira, H.; Oshima, M. *Phys. Rev. B*, **2009, 79**: 113103

15 Blennow, P.; Hagen, A.; Hansen, K. K.; Wallenberg, L. R.; Mogensen, M. *Solid State Ionics*, **2008, 179**: 2047

16 Page, K.; Kolodiazhnyi, T.; Proffen, T.; Cheetham, A. K.; Seshadri, R. *Phys. Rev. Lett*., **2008, 101**: 205502

17 Guo, X. G.; Chen, X. S.; Sun, Y. L.; Sun, L. Z.; Zhou, X. H.; Lu, W. *Phys. Lett. A*, **2003, 317**: 501

18 Evarestov, R. A.; Piskunov, S.; Kotomin, E. A.; Borstel, G. *Phys. Rev. B*, **2003, 67**: 064101

19 Hihuchi, T.; Tsukamoto, T.; Sata, N.; Ishigame, M.; Tezuka, Y.; Shin, S. *Phys. Rev. B*, **1998, 57**: 6978

20 Dai, S.; Lu, H.; Chen, F.; Chen, Z.; Ren, Z. Y.; Ng, D. H. L. *Appl. Phys. Lett*., **2002, 80**: 3545

21 Guo, H.; Liu, L.; Fei, Y.; Xiang, W.; Lu, H.; Dai, S.; Zhou, Y.; Chen, Z. *J. Appl. Phys*., **2003, 94**: 4558

22 Hohenberg, P.; Kohn, W. *Phys. Rev. B*, **1964, 136**: 864

23 Vanderbilt, D. *Phys. Rev. B*, **1990, 41**: 7892

24 Perdew, J. P.; Chevary, J. A.; Vosko, S. H.; Jackson, K. A.; Pederson, M. R.; Singh, D. J.; Fiolhais, C. *Phys. Rev. B*, **1992, 46**: 6671

25 Monkhorst, H. J.; Pack, J. D. *Phys. Rev. B*, **1976, 13**: 5188

26 Pfrommer, B. G.; Cote, M.; Louie, S. G.; Cohen, M. L. *J. Comput. Phys*., **1997, 131**: 233

27 Xiao, B.; Feng, J.; Zhou, C. T.; Xing, J. D.; Xie, X. J.; Chen, Y. H. *Chem. Phys. Lett*., **2008, 459**: 129

28 Van Benthem, K.; Elsassser, C.; French, R. H. *J. Appl. Phys*., **2001, 90**: 6156

29 Sham, L. J.; Schluter, M. *Phys. Rev. Lett*., **1983, 51**: 1888

30 Zhang, F. C.; Zhang, Z. Y.; Zhang, W. H.; Yan, J. F.; Yun, J. N. *Acta Phys. -Chim. Sin*., **2009, 25**: 61 [张富春, 张志勇, 张威虎, 闫军锋, 负江妮. 物理化学学报, **2009, 25**: 61]

31 Higuchi, T.; Tsukamoto, T.; Yamaguchi, S.; Kobayashi, K.; Sata, N.; Ishigame, M.; Shin, S. *Nucl. Instrum. Methods Phys. Res. Sect. B-Beam Interact. Mater. Atoms*, **2003, 199**: 255

32 Higuchi, T.; Tsukamoto, T.; Sata, N.; Ishigame, M.; Kobayashi, K.; Yamaguchi, S.; Shin, S. *Solid State Ionics*, **2002, 154–155**: 735

33 Burstein, E. *Phys. Rev*., **1954, 93**: 632

34 Mahan, G. D. *J. Appl. Phys*., **1980, 51**: 2634

35 Saha, S.; Sinha, T. P.; Mookerjee, A. *Phys. Rev. B*, **2000, 62**: 8828